

# Structural Integrity Evaluation of Generator Retaining Ring at Dieng Geothermal Power Plant

Hilman Syaeful Alam, Imam Djunaedi, Aditya Sukma Nugraha, and Demi Soetraprawata

**Abstract**—The structural integrity of generator retaining ring at Dieng geothermal power plant has been evaluated using analytical and finite element method base on the scenario of the over speed at 100%, 120% and 150% of rated speed. To validate the evaluation, penetrant testing is applied with the retaining ring remains patches to its rotor. Base on the evaluation results of both methods, safety factor against yielding is greater than 1.0. Then based on the penetrant testing, it was not detected the presence of defects on the retaining ring generator surface. However from the displacement result which obtained by finite element, the displacement in third case has the same value as the interference therefore there is a possibility of retaining ring movement from its position that can lead to fretting failure.

**Index Terms**—Generator retaining ring, structural integrity, finite elements, safety factor.

## I. INTRODUCTION

Generator retaining rings are normally the most highly stressed component of the generator and possibly the highest stressed component of the entire turbine generator set. The function of the retaining rings is to retain the end winding coil assembly, insulation material and packing blocks against centrifugal forces developed when the rotor is rotating. The shrink-fitted joint method by thermal expansion and contraction of metal is used to mount the retaining ring on the generator rotor [1]. The fits at the retaining ring must be designed with sufficient interference to keep them tight up to at least 120% rated speed [2]. The shrink-fitted method is a commonly used to assemble parts in mechanical application. Advantages are high rigidity, compactness, lightweight, reliable and non-expensive manner. However, the contact separation and failure occurrences for those common systems have been more rarely addressed in the literature [3]-[8]. Under cyclic bending or torsion loads, fretting could occur at the edge of the shaft-hub fitting surface. Fretting is a wear/corrosion mechanism resulting from the slight relative movement of contacting surfaces [8]. In the case of generator retaining rings, fretting can develop at shrink fit and mating

surfaces and at winding support positions. The high levels of residual stress from the cold working process and further loads which are imposed by shrink fitting, self-weight and copper support loads during operation can lead to service failure. The failure on the generator retaining ring can result in a catastrophic failure of the generator and part of its associated turbine or prime mover. It is possible for these rings to rupture or explode damaging the stator end winding, rotor windings and end covers.

One of the geothermal power plants in Indonesia is Dieng, with installed capacity of 60 MW. Geographically, the plant is located in Dieng Plateau, under the administrative district of Wonosobo, Central Java, Indonesia. The plant was built in 1995 with commissioning in 1998. In 2013, the plant was reported suffered damage due to malfunctioning of the flow control system causing the over flow of working fluid. There are damages to some components, i.e. the turbine and generator rotor. In the generator rotor, damage occurs on the bearing and labyrinth seal, which is thought to be caused by high vibration due to over speed. In addition these components damages, it is feared the damage also occurred in the generator retaining ring. However, based on the visual inspection, it didn't find any damage and flaw on the retaining ring.

To ensure the structural integrity of the retaining ring, the more precise inspections and evaluation is required when compared with the visual. Traditionally, the inspections of retaining ring flaws require the removal of the retaining ring from the rotor. This operation has major implications of damage risk, cost, safety and time. To overcome this problem, the structural integrity of retaining ring is evaluated using analytical and numerical method. Nowadays, numerical methods such as finite element method (FEM) have become widespread in order to evaluate the stresses and deformations by considering the actual geometry and working conditions. The application of finite element to analyze the shrink-fitted joint has been performed on the literature [9]-[16]. In this study, the structural integrity of retaining ring is evaluated base on the scenario of the over speed due to over flow of the working fluid at 100%, 120% and 150% of the operating speed. To validate the analytical and finite element calculations, Non Destructive Test (NDT), i.e. Penetrant Testing (PT) is applied with the retaining ring remains patches to its rotor.

## II. MATERIALS AND METHODS

The Generator at Dieng geothermal power plant was installed in 1995 with rating generator 75000 KVA, Voltage 15000 Volts, Current 2887 Amp, and Rpm 3000. The rotor has two poles of winding, both leads position on the exciter

Manuscript received May 10, 2014; revised August 30, 2014. This work was supported in part by the Indonesian Institute of Sciences and PT. Geo Dipa Energy (Dieng Geothermal Power Plant).

Hilman Syaeful Alam and Demi Soetraprawata are with the Technical Implementation Unit for Instrumentation Development, Indonesian Institute of Sciences, Jl, Sangkuriang Komp, LIPI Gd. 30, Bandung, 40135, Indonesia (e-mail: hilm003@lipi.go.id, demistp@gmail.com).

Imam Djunaedi is with Research Center of Physics, Indonesian Institute of Sciences, Jl, Sangkuriang Komp, LIPI Gd. 80, Bandung, 40135, Indonesia (e-mail: imam\_djunaedi@yahoo.com).

Aditya Sukma Nugraha is with the Research Center for Power and Mechatronics, Indonesian Institute of Sciences, Jl, Sangkuriang Komp, LIPI Gd. 20, Bandung, 40135, Indonesia (e-mail: aditngrh@gmail.com).

side disconnected to the diodes and exciter armature. Fig. 1 shows the generator rotor assembly and the position of the retaining ring on both sides, i.e. the turbine and exciter side, while Fig. 2 shows the surface condition of the retaining ring which is visually no visible signs of a flaw or defect. Analytical calculation and finite element simulation are subsequently used to evaluate the structural integrity of the retaining ring in which two of the evaluation results will be compared with results of the Penetrant Testing (PT).

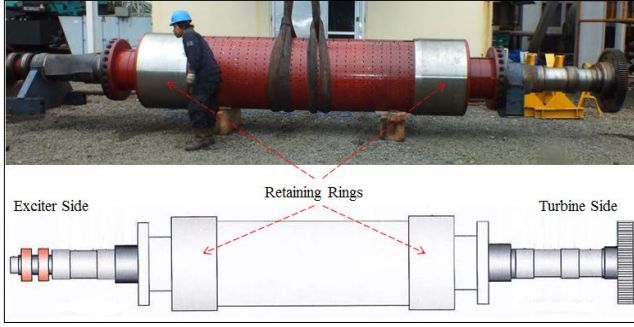


Fig. 1. Rotor generator of Dieng geothermal power plant.



Fig. 2. No marks on retaining ring surface.

#### A. Analytical Calculations of Retaining Ring Integrity

Fig. 3 shows a schematic of the shrink-fit joint between the retaining ring and the shaft. The stress around the hub or the retaining ring must not be so great to cause the material to yield, even in the presence of other stress in the system, including axial, torsional, bending, shear, pressure, thermal, and inertial stress. The first two types of stresses often rely on the interference fit itself to transfer them across the joint, thus they directly affect the minimum required interference fit pressure. Bending stress can be equated to axial stresses at the joint interface and generally are only significant if a radial support is located far from the joint. Shear force stresses act to decrease the radial dimensions of the parts and can thus cause loosening of the joint. Thermal stresses can cause a part to come loose or split apart. Inertial stresses can also cause the part to come loose or split [17].

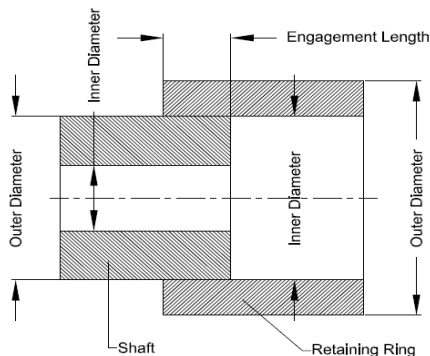


Fig. 3. Schematic of shrink fit joint between the retaining ring and shaft.

Therefore the stress analysis and integrity evaluation of retaining ring according to [17], [18] by neglecting the effect due to bending stress use the following procedure.

The differential thermal radial interference due to different operation and assembly temperatures for different materials  $u_{thermal}$  can be expressed as follows:

$$u_{thermal} = \Delta T(\alpha_s - \alpha_h)D_{hi}/2 \quad (1)$$

where  $\Delta T$  is the temperature difference between operating and assembly conditions,  $\alpha_s$  is the thermal expansion coefficient of shaft,  $\alpha_h$  is the thermal expansion coefficient of hub, and  $D_{hi}$  is the hub inner diameter.

The differential radial interference due to Poisson's effect of axial force  $u_{poisson}$  can be expressed as follows:

$$u_{poisson} = \frac{2Fv_h D_{hi}}{\pi(D_{ho}^2 - D_{hi}^2)E_h} - \frac{2Fv_s D_{so}}{\pi(D_{so}^2 - D_{si}^2)E_s} \quad (2)$$

where  $F$  is the axial force to be transmitted,  $v_h$  is the Poisson's ratio of hub,  $v_s$  is the Poisson's ratio of shaft,  $D_{ho}$  is the hub outer diameter,  $D_{so}$  is the shaft outer diameter,  $D_{si}$  is the shaft inner diameter,  $E_h$  is the hub elastic modulus and  $E_s$  is the shaft elastic modulus.

The hub radial displacement due to rotation  $u_{h,cf}$  can be expressed as follows:

$$u_{h,cf} = \frac{\rho_h \omega^2 (1 - \nu_h^2)}{8E_h} \left[ - \left( \frac{D_{hi}}{2} \right)^3 + (3 + \nu_h) \left\{ \frac{(D_{ho}^2 + D_{hi}^2)}{4(1 + \nu_h)} \left( \frac{D_{hi}}{2} \right) + \frac{(D_{ho}^2 D_{hi}^2)}{8(1 - \nu_h)} \right\} \right] \quad (3)$$

where  $\rho_h$  is the density of the hub material and  $\omega$  is the rotational speed.

The shaft radial displacement due to rotation  $u_{s,cf}$  can be expressed as follows:

$$u_{s,cf} = \frac{\rho_s \omega^2 (1 - \nu_s^2)}{8E_s} \left[ - \left( \frac{D_{so}}{2} \right)^3 + (3 + \nu_s) \left\{ \frac{(D_{so}^2 + D_{si}^2)}{4(1 + \nu_s)} \left( \frac{D_{so}}{2} \right) + \frac{(D_{si}^2 D_{so}^2)}{8(1 - \nu_s)} \right\} \right] \quad (4)$$

where  $\rho_s$  is the density of the shaft material.

The maximum diametrical interference  $\Delta$  can be expressed as follows:

$$\Delta = (D_{so} + \Delta_{s,+tol}) - (D_{ho} + \Delta_{h,-tol}) + 2(u_{poisson} + u_{thermal} + u_{s,cf} - u_{h,cf}) \quad (5)$$

where  $\Delta_{s,+tol}$  is the outside diameter upper deviation of shaft and  $\Delta_{h,-tol}$  is the inside diameter lower deviation of hub.

Therefore, the interference pressure as a result of diametrical interference,  $P$ :

$$P = \frac{\Delta}{\frac{D_{hi}}{E_h} \left( \frac{D_{ho}^2 + D_{hi}^2}{D_{ho}^2 - D_{hi}^2} + \nu_h \right) + \frac{D_{so}}{E_s} \left( \frac{D_{so}^2 + D_{si}^2}{D_{so}^2 - D_{si}^2} - \nu_s \right)} \quad (6)$$

The radial stress on hub due to interference pressure  $\sigma_{r,p}$  can be expressed as follows:

$$\sigma_{r,p} = -P \quad (7)$$

The circumferential stress on hub due to interference pressure  $\sigma_{\theta,p}$  can be expressed as follows:

$$\sigma_{\theta,p} = P \left( \frac{D_{ho}^2 + D_{hi}^2}{D_{ho}^2 - D_{hi}^2} \right) \quad (8)$$

The axial stress on hub due to axial force  $\sigma_z$  can be expressed as follows:

$$\sigma_z = \frac{4F}{\pi(D_{ho}^2 + D_{hi}^2)} \quad (9)$$

The shear stress on hub caused by torque  $\tau$  can be expressed as follows:

$$\tau = \frac{16TD_{hi}}{\pi(D_{ho}^4 - D_{hi}^4)} \quad (10)$$

where  $T$  is the torque to be transmitted.

The circumferential stress on hub due to centrifugal effect  $\sigma_{\theta,cf}$  can be expressed as follows:

$$\sigma_{\theta,cf} = \frac{\rho\omega^2(3+v_h)}{8} \left( \frac{D_{hi}^2}{4} + \frac{D_{ho}^2}{2} - \frac{1+3v_h}{3+v_h} \frac{D_{hi}^2}{4} \right) \quad (11)$$

Therefore the Von Mises stress at the hub surface,  $\sigma_{VM}$  can be expressed as follows:

$$\sigma_{VM} = \sqrt{\frac{(\sigma_r - \sigma_{\theta,press} - \sigma_{\theta,cf})^2 + (\sigma_{\theta,press} + \sigma_{\theta,cf} - \sigma_z)^2 + (\sigma_r - \sigma_z)^2}{2} + 3\tau^2} \quad (12)$$

### B. Finite Element Method

In this study, the results of stress analysis using analytical methods are validated using ANSYS based on the 3D finite element method. The geometry of retaining rings is modeled which based on the actual dimensions using ANSYS Design Modeler and the results can be seen in Fig. 4(a). After geometry modeling and material definition, the next stage in simulation is a meshing of 3D solid of retaining rings. Meshing is dividing the components into smaller elements which are then analyzed according to the material properties, the boundary conditions and the loading conditions. Based on the results of meshing, it is generated 45066 element and 85137 nodes that are shown in Fig. 4(b). The settings of boundary condition which occurs on the retaining ring are similar with the analytical procedure, which is due to axial tension, torsion, shear, pressure, thermal, and inertial. Therefore the safety factor is calculated based on the yield strength of the material or the ratio between the yield strength and Von Mises stress of the retaining ring.

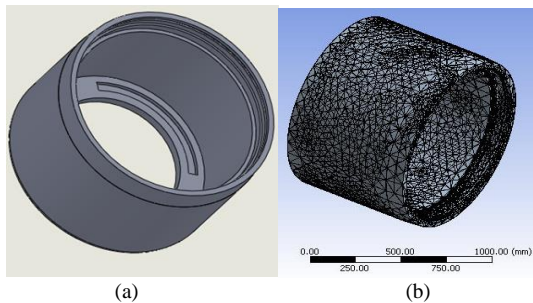


Fig. 4. 3D modeling of the retaining ring.

### C. Inspection of the Retaining Ring

For the outer surface of the retaining ring, pitting and cracking would be detected by using a liquid dye penetrant. Testing is done by applying a dye penetrant on the surface of retaining ring at 5 minutes of dwell time. During that interval, the liquid penetrant entered on the surface which has the defect, while the penetrant which is not entered on a surface

that has no defect is cleaned. Further, a developer is used to describe the profile of defects on the material. In this study, it is used the SKL-SP type of penetrant from Magnaflux with SKD-2 developer type and SKC-S remover type.

## III. RESULTS AND DISCUSSIONS

The structural integrity of the retaining ring is evaluated base on the scenarios of the over-speed at 100%, 120% and 150% of the operating speed. The parameters as the input on the analysis for the retaining ring and the shaft can be seen respectively in Table I and Table II. Based on the data of the inside diameter of retaining ring and the outside diameter of the shaft, it is produced the interference of 2.2 mm, therefore the deformation of the retaining ring is limited to half of the value of the interference. Based on the ratio between the diameter and the thickness of the retaining ring, the analytical calculation is performed by the stress analysis for thin walled tubes. The retaining ring is made from 18Cr5Mn material which has the yield strength  $S_y$  887.354 MPa. The yield strength of the material is used to determine the criteria of retaining ring failure in receiving a total stress or Von Mises stress.

TABLE I: RETAINING RING/HUB PARAMETER

| Parameter                                          | Value     | Unit              |
|----------------------------------------------------|-----------|-------------------|
| Hub outside diameter, $D_{ho}$                     | 898       | mm                |
| Hub inside diameter, $D_{hi}$                      | 835.8     | mm                |
| Inside diameter upper deviation, $\Delta_{h,+tol}$ | 0.004     | mm                |
| Inside diameter lower deviation, $\Delta_{h,-tol}$ | 0         | mm                |
| Stress concentration factor, $K_t$                 | 2         |                   |
| Modulus of elasticity, $E_h$                       | 207       | GPa               |
| Yield strength, $S_y$                              | 887.354   | MPa               |
| Poisson's ratio, $\nu_h$                           | 0.4       |                   |
| Coefficient of thermal expansion, $\alpha_h$       | 0.0000117 | m/m°C             |
| Density, $\rho_h$                                  | 7.833     | g/cm <sup>3</sup> |

TABLE II: SHAFT PARAMETERS

| Parameter                                           | Value     | Unit              |
|-----------------------------------------------------|-----------|-------------------|
| Shaft outside diameter, $D_{ho}$                    | 838       | mm                |
| Shaft inside diameter, $D_{hi}$                     | 0         | mm                |
| Outside diameter upper deviation, $\Delta_{h,+tol}$ | 0.009     | mm                |
| Outside diameter lower deviation, $\Delta_{h,-tol}$ | 0         | mm                |
| Stress concentration factor, $K_t$                  | 2         |                   |
| Modulus of elasticity, $E_h$                        | 207       | GPa               |
| Yield strength, $S_y$                               | 552       | MPa               |
| Poisson's ratio, $\nu_h$                            | 0.27      |                   |
| Coefficient of thermal expansion, $\alpha_h$        | 0.0000117 | m/m°C             |
| Density, $\rho_h$                                   | 7.833     | g/cm <sup>3</sup> |

The working conditions of the retaining ring as the input of the analytical calculation and the finite element analysis can be seen in Table III. All these data will be evaluated based on the scenario of the over-speed at 100%, 120% and 150% of the operating speed or in 3000, 3600 and 4500 rpm.

TABLE III: WORKING CONDITIONS

| Parameter                          | Value  | Unit |
|------------------------------------|--------|------|
| Torque to be transmitted, $T$      | 238854 | Nm   |
| Axial force to be transmitted, $F$ | 27940  | N    |
| Coefficient of friction, $\mu$     | 0.15   |      |
| Operation temperature, $T_o$       | 40     | °C   |
| Engagement length, $L$             | 61     | mm   |

Based on the analytical calculations procedure of the retaining ring integrity and from the equations (1) until (12), the analytical calculation results can be seen in Table IV. From the analytical result, the radial displacement of retaining ring for case 1, 2 and 3 respectively are 0.50, 0.70 and 0.81 mm, therefore is below the half of the interference value and still meet the requirements. The interference pressure due to the influence of thermal, the Poisson's effect of axial force and the displacement of the hub and shaft at the three cases indicates that the higher the rotation of over-speed, the lower the interference pressure, its mean that the power of the shrink-fit connection will be even lower. It can be seen also from the declining of the radial and circumferential stress. The axial stress and shear stress doesn't change for all three cases, because the axial load and torque which are transmitted are the same for all three cases. However, the centrifugal stress has increased significantly with the increasing of rotational speed. The influence of the centrifugal stress has a significant impact on the results of the Von Mises or equivalent stress calculations. The Von Mises stress on the retaining ring for case 1, 2 and 3 respectively are 555.0, 571.1, and 594.4 MPa, while the yield strength of the retaining ring material i.e. 18Cr5Mn is 887.354 MPa, so the safety factor against yielding for case 1, 2 and 3 are 1.59, 1.55,

and 1.49. Therefore, based on the results of the stress analysis using analytical methods, the possibility of failure on the retaining ring due to plastic deformation was not found, because the safety factor is above 1.0.

The results of stress analysis using the analytical method are then validated using ANSYS simulation based on 3D finite element method. Fig. 5 shows the finite element simulation results for displacement for three cases. For case 1 and 2, the both displacement value is below the half of the interference value therefore it still meets the requirements. However, the displacement of case 3 has the same value as the interference therefore there is a possibility of retaining ring movement from its position. Fig. 6 shows the Von Mises stress for each case. The maximum Von Mises stress is in the region of shrink fit joint in the all three cases, that for case 1, 2 and 3 respectively are 407.01, 470.43, and 517.1 MPa. Based on these results, there is a difference between stress analysis using analytical and finite element. In general, the results which obtained by finite element for the three case are smaller when compared with the analytical, with the difference for case 1, 2 and 3, respectively are 26.7%, 17.6% and 13.0% smaller than the analytical method. Therefore the safety factor which obtained using the finite element will be greater than the analytical method.

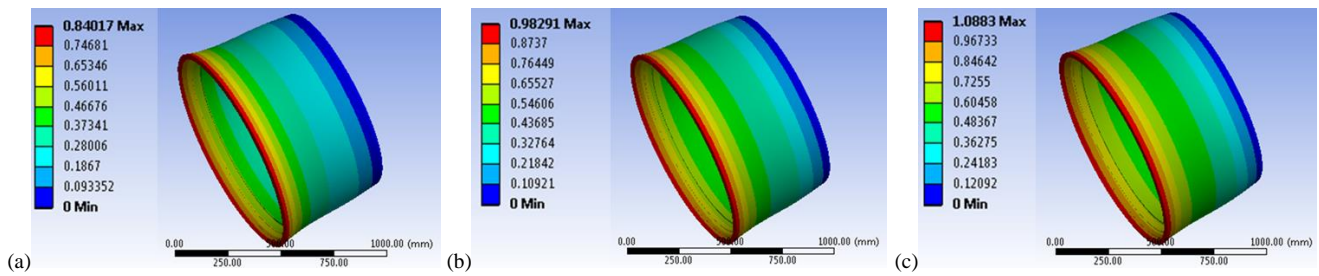


Fig. 5. The displacement in mm for (a) Case 1, (b) Case 2 and (c) Case 3.

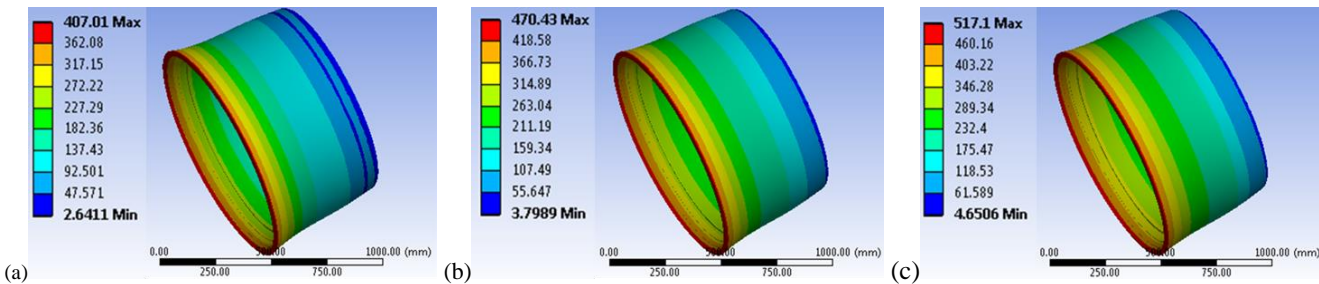


Fig. 6. Von misses stress in MPa for (a) Case 1, (b) Case 2 and (c) Case 3.

TABLE IV: ANALYTICAL CALCULATION RESULTS

| Parameter                                                                       | Case 1           | Case 2           | Case 3           | Unit |
|---------------------------------------------------------------------------------|------------------|------------------|------------------|------|
|                                                                                 | 100% rated speed | 120% rated speed | 150% rated speed |      |
| Hub Radial Displacement, $u_{h,cf}$                                             | 0.50             | 0.70             | 0.81             | mm   |
| Interference pressure, $P$                                                      | 27.8             | 24.3             | 17.4             | MPa  |
| Radial stress, $\sigma_{r,pressure}$                                            | -27.8            | -24.3            | -17.4            | MPa  |
| Circumferential stress due to interference pressure, $\sigma_{\theta,pressure}$ | 387.9            | 339.6            | 243.5            | MPa  |
| Axial stress, $\sigma_z$                                                        | 0.3              | 0.3              | 0.3              | MPa  |
| Shear stress, $\tau$                                                            | 6.3              | 6.3              | 6.3              | MPa  |
| Circumferential stress due to centrifugal effect $\sigma_{\theta,cf}$           | 152.7            | 219.0            | 342.1            | MPa  |
| Max Von Mises stress, $\sigma_{VM}$                                             | 555.0            | 571.1            | 594.4            | MPa  |
| Factor of safety against yielding                                               | 1.59             | 1.55             | 1.49             |      |

Fig. 7 shows the results of finite element simulations for minimum safety factor at case 1, 2, and 3 which are 2.1, 1.9, and 1.7 respectively. The difference of minimum safety factor for case 1, 2 and 3 are respectively 81.8%, 88.6% and

145.1% greater than the analytical method. The magnitudes of the minimum safety factor in all three cases indicate that the value has declined, in proportion to the increase of rotational speed. However, based on both analytical and

finite element, the minimum safety factor against yielding is greater than 1.0, therefore the retaining ring components are in a safe condition to the plastic deformation of the material.

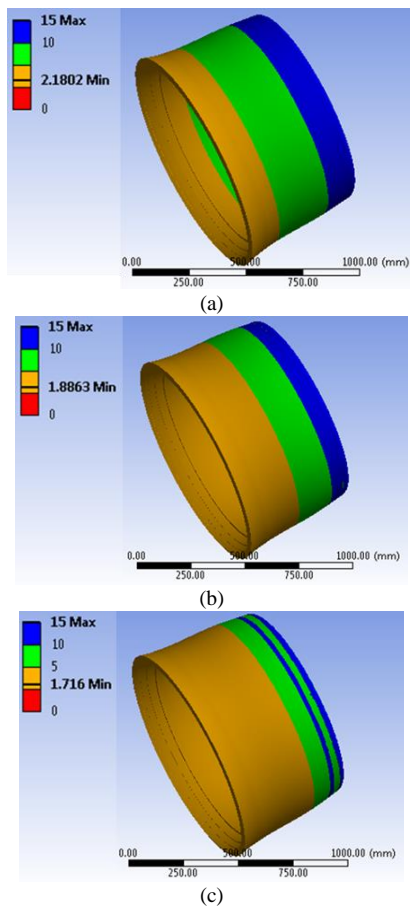


Fig. 7. Factor of Safety against yielding for (a) Case 1, (b) Case 2 and (c) Case 3.



Fig. 8. The inspection result of penetrant testing (PT).

To validate the analytical and finite element calculations, Penetrant Testing (PT) is applied on both the retaining ring, which is on the exciter side and turbine side. In this study, PT performed on the entire outer surface of the retaining ring, which inspection results can be seen in Fig. 8. Based on this inspection, it was not detected the presence of defects on both sides of the retaining ring generator (turbine and exciter side).

#### IV. CONCLUSION

Base on the evaluation of the retaining ring integrity using analytical and finite element method with the three case of 100%, 120% and 150% of rated speed, safety factor against

yielding is greater than 1.0 thus the retaining ring components are in a safe condition to the plastic deformation of the material. Then based on the penetrant testing, it was not detected the presence of defects on both sides of the retaining ring generator (turbine and exciter side). However from the displacement result which obtained by finite element, the displacement in third case has the same value as the interference therefore there is a possibility of retaining ring movement from its position that can lead to fretting failure.

#### ACKNOWLEDGMENT

The authors would like to thank to Research Center for Power and Mechatronics, Indonesian Institute of Sciences, for facilitating the finite element simulation using ANSYS. Moreover thanks to PT. Geo Dipa Energy and all the team members of energy research, Indonesian Institute of Sciences for any assistance that has been given.

#### REFERENCES

- [1] Working Group A1.16, Conseil Internationale des Grands Reseaux Electriques, *Generator End-Winding Retaining Rings—a Literature Survey and Care Guideline*, CIGRE Publication, 2010.
- [2] S. H. Hwang and J. S. Choi, "Analysis of shrink-fitted retaining ring on rotor body in generator," in *Proc. ABAQUS Users' Conference*, 2004, pp. 359-372.
- [3] R. Gutkin and B. Alfredsson, "Growth of fretting fatigue cracks in a shrink-fitted joint subjected to rotating bending," *Engineering Failure Analysis*, vol. 15, pp. 582-596, 2008.
- [4] N. Antoni, "Contact separation and failure analysis of a rotating thermo-elastoplastic shrink-fit assembly," *Applied Mathematical Modelling*, vol. 37, pp. 2352-2363, 2013.
- [5] J. Juoksukangas, A. Lehtovaara, and A. M. äntyl ä "The effect of contact edge geometry on fretting fatigue behavior in complete contacts," *Wear*, vol. 308, pp. 206-212, 2013.
- [6] T. Juuma, "Torsional fretting fatigue strength of a shrink-fitted shaft with a grooved hub," *Tribology International*, vol. 33, pp. 537-543, 2000.
- [7] B. Alfredsson, "Fretting fatigue of a shrink-fit pin subjected to rotating bending: Experiments and simulations," *International Journal of Fatigue*, vol. 31, pp. 1559-1570, 2009.
- [8] F. Zeng, Z. B. Cai, Z. Q. Feng, and Z. R. Zhou, "In situ observation and analysis of a shrink-fitted PMMA shaft subjected to rotating bending," *Tribology International*, vol. 48, pp. 149-154, 2012.
- [9] D. Hao and D. Wang, "Finite-element modeling of the failure of interference-fit planet carrier and shaft assembly," *Engineering Failure Analysis*, vol. 33, pp. 184-196, 2013.
- [10] A. Rusin, G. Nowak, and W. Piecha, "Shrink connection modelling of the steam turbine rotor," *Engineering Failure Analysis*, vol. 34, pp. 217-227, 2013.
- [11] F. Lanoue, A. Vadean, and B. Sanschagrin, "Fretting fatigue strength reduction factor for interference fits," *Simulation Modelling Practice and Theory*, vol. 19, pp. 1811-1823, 2011.
- [12] H. Boutoutaou, M. Bouaziz, and J. F. Fontaine, "Modelling of interference fits with taking into account surfaces roughness with homogenization technique," *International Journal of Mechanical Sciences*, vol. 69, pp. 21-31, 2013.
- [13] M. Y. Sun, S. P. Lu, D. Z. Li, Y. Y. Li, X. G. Lang, and S. Q. Wang, "Three-dimensional finite element method simulation and optimization of shrink fitting process for a large marine crankshaft," *Materials and Design*, vol. 31, pp. 4155-4164, 2010.
- [14] V. Kovan, "Separation frequency analysis of interference fitted hollow shaft-hub connections by finite element method," *Advances in Engineering Software*, vol. 42, pp. 644-648, 2011.
- [15] A. Ozel, S. Temiz, M. D. Aydin, and S. Sen, "Stress analysis of shrink-fitted joints for various fit forms via finite element method," *Materials and Design*, vol. 26, pp. 281-289, 2005.
- [16] H. Boutoutaou, M. Bouaziz, and J. F. Fontaine, "Modeling of interference fits taking form defects of the surfaces in contact into account," *Materials and Design*, vol. 32, pp. 3692-3701, 2011.
- [17] A. H. Slocum, *Precision Machine Design*, Society of Manufacturing Engineers, Dearborn MI, Prentice Hall, 1995, pp. 384-393.
- [18] Ames website. (2013). Interference (press & shrink) fit calculator [Online]. Available:

<http://www.amesweb.info/InterferenceFit/InterferenceFitCalculationSteps.aspx>



**Hilman Syaeful Alam** received his B.S. degree in mechanical engineering from Jenderal Achmad Yani University, Indonesia in 2003 and M.S. degree in mechanical engineering from Institut Teknologi Bandung, Indonesia in 2010. He is working as a researcher at Indonesian Institute of Sciences (LIPI) from 2006 until now. His research areas are renewable energy, engineering design, solid mechanics, instrumentation, finite element and computational fluid dynamics.



**Imam Djunaedi** received his B.S. degree in mechanical engineering from Institut Teknologi Bandung, Indonesia in 1984. He had been working as a Ph.D. research student at School of Computer & Electrical Engineering Curtin University of Technology, Australia from 1993 to 1996. He is working as a researcher at Indonesian Institute of Sciences (LIPI) from 1986 until now. His research areas are renewable energy, optimization, mechatronics, thermal engineering and power plant.



**Adit Sukma Nugraha** received his B.S. degree in mechanical engineering from Diponegoro University, Indonesia in 2006 and M.S. degree in mechanical engineering from Institut Teknologi Bandung, Indonesia in 2014. He worked as a researcher at Indonesian Institute of Sciences (LIPI) from 2008 until now. His research areas are mechatronics, vibration, and renewable energy.



**Demi Soetraprawata** received his B.S. degree in physics from Nasional University, Indonesia in 1996 and M.S. degree in instrumentation and control from Institut Teknologi Bandung, Indonesia in 2014. He is working as a researcher at Indonesian Institute of Sciences (LIPI) from 1983 until now. His research areas are instrumentation and control.